DOI: 10.1002/((please add manuscript number))
Article type: Communication

Large efficiency improvement in $Cu_2ZnSnSe_4$ solar cells by introducing a superficial Ge nano-layer

*Sergio Giraldo, Markus Neuschitzer, Thomas Thersleff, Simón López-Marino, Yudania Sánchez, Haibing Xie, Mónica Colina, Marcel Placidi, Paul Pistor, Victor Izquierdo-Roca, Klaus Leifer, Alejandro Pérez-Rodríguez, and Edgardo Saucedo**

S. Giraldo[1], M. Neuschitzer[1], Dr. T. Thersleff[2], S. López-Marino[1], Y. Sánchez[1], H. Xie[1], Dr. M. Colina[1], Dr. M. Placidi[1], Dr. P. Pistor[1], Dr. V. Izquierdo-Roca[1], Prof. K. Leifer[2], Prof. A. Pérez-Rodríguez[1,3], and Dr. E. Saucedo[1]

[1]Catalonia Institute for Energy Research, (IREC), Jardins de les Dones de Negre 1, 08930 Sant Adrià del Besòs (Barcelona), Spain.
[2]The Ångström Laboratory, Department of Engineering Sciences, Uppsala University, Box 534, Uppsala, Sweden.
[3]IN2UB, Universitat de Barcelona, c. Martí i Franquès 1, 08028 Barcelona, Spain.

E-mail: esaucedo@irec.cat

Keywords: $Cu_2ZnSnSe_4$, Ge nano-layer, Kesterite, thin film solar cells

As the knowledge on kesterite photovoltaic absorbers increases, the factors limiting the efficiency of solar cells based on this family of materials become more and more evident.[1] Comparing the best efficiencies obtained using $Cu_2ZnSn(S,Se)_4$ (CZTSSe) as absorber with more mature CdTe and $Cu(In,Ga)Se_2$ (CIGSe) technologies, it is clear that the voltage deficit is the major challenge that kesterite based solar cells have to face in the near future.[2] Recently, the pure selenide $Cu_2ZnSnSe_4$ (CZTSe) compound has demonstrated efficiencies exceeding 11%, with an open circuit voltage (V_{OC}) of 423 mV.[3] Commonly, the highest efficiencies were reported for kesterites with Se rich sulfo-selenide solid solutions, which generally lead to a higher V_{OC}. This highlights the importance to identify and reduce the voltage losses for these materials.[2,4] In this sense, and with the aim to solve the inherent problems of kesterites, the substitution of cations has been explored in some extent.[5-8] In particular, Sn exhibits an intrinsic multi-charge character and thus, the Sn-site substitution is probably the most interesting.[5,9] This is because multi-charge atoms commonly introduce

deep defects that increase the non-radiative charge carrier recombination. This has an especially severe impact on the degradation of the V_{OC}.[5,9]

For this reason, one of the most interesting approaches is to substitute Sn by other cations such as Ge. By alloying CZTSe with Ge the band-gap can be tuned from 1.0 eV (pure Sn/Zn kesterite) to 1.35 eV (pure Ge/Zn kesterite).[10,11] Additionally, several other beneficial effects have been associated with the use of Ge, like the increase of carrier lifetime and the suppression of Sn^{+2} state formation.[5,6] Nevertheless till now, the use of Ge has demonstrated rather limited devices improvements with respect to the pure Sn kesterite. Furthermore, all reports published so far are based on the use of large Ge amounts, which may compromise the viability of this technological approach, as Ge has been identified as a critical raw material with an earth crust abundance about 1.6 ppm, but also because is a scattered material disabling the extraction by mining.[12] For example, Kim et al. reported an increase of the devices efficiency from 4.6% to 6.0% using a graded band gap by alloying Cu_2ZnSnS_4 with Ge, observing a Ge/(Sn+Ge) ratio about 0.50 at the surface and an almost pure Ge phase at the back.[7] The efficiency improvement is mainly explained by an increase of the J_{SC}, and the reported values are far from the state-of-the-art efficiencies reported for kesterite solar cells. Bag et al. reported the Ge substitution in CZTSe solar cells, too, obtaining a rather small efficiency improvement (from 9.07% for the pure Sn kesterite to 9.14% for the Sn-Ge alloyed with 40% of Ge), but observing a remarkable increase of the V_{OC} in more than 50 mV.[5] Finally, Hages et al. reported an improved performance of Ge-alloyed $Cu_2Zn(Sn,Ge)(S,Se)_4$ solar cells, increasing the efficiency from 8.4% (no Ge) to 9.4% (with 30% of Ge), mainly explained by the increase of 50 mV in the V_{OC}.[6] This shows that till now although very promising, attempts of alloying kesterite with large amounts of Ge has demonstrated rather small improvements in the solar cell performance.

In this work, we report a breakthrough in kesterite based technologies. We demonstrate that high-voltage and high-efficiency devices can be easily achieved using small quantities of Ge,

leading to efficiencies higher than 10%. The Ge-based approach presented here is based on the evaporation of a 10nm thick Ge layer on top of the Cu/Sn/Cu/Zn metallic precursor stack prior to the selenization step, using a sequential process to synthesize CZTSe absorbers.[13] As will be shown later, this leads to a substitution of less than 1.6% of Sn in the final kesterite structure, ensuring the sustainability of the developed processes.

To analyze the impact of Ge on the optoelectronic properties of the devices, in the following we first present the impact of the superficial Ge nano-layer on the devices parameters in a J-V and external quantum efficiency (EQE) comparison. The morphology, elemental composition and distribution of the resulting absorber layers will be evaluated by scanning electron microscopy (SEM), time-of-flight secondary ion mass spectroscopy (TOF-SIMS) and by combining transmission electron microscopy (TEM) with electron energy loss spectroscopy (EELS). Finally in the supporting information (S.I.) we present a detailed characterization of the back and front surface of the CZTSe absorbers with and without Ge-layer by Raman spectroscopy, and of the surface with X-ray photoemission spectroscopy (XPS).

Figure 1 (left) presents the J-V illuminated curves of the reference cell (Sn-pure CZTSe) and those produced introducing a 10 nm thick Ge layer on top of the precursor (Ge10) as is described in the Experimental Section. This corresponds to a Ge/(Ge+Sn) ratio of 0.044, i.e. a 4.4% of nominal Sn substitution by Ge. In the right side of **Figure 1,** the corresponding external quantum efficiency is plotted, including the reflectivity of the complete devices. Notably, the efficiency increases from 7% (reference CZTSe) to 10.1% (Ge10) representing the highest efficiency reported till now for a Ge containing cell, with a remarkable improvement of all the optoelectronic parameters (see Table 1 in **Figure 1**). In fact, the maximum efficiency was achieved with a 10 nm thick Ge nano-layer on top, but the whole range between 0 nm to 25 nm has been explored in a first optimization as is presented in the S.I. It is important to remark the large improvement in the V_{OC}, from 409 mV for the reference cell to 453 mV for the record one, although some cells produced in other rounds

have achieved a V_{OC} as high as 469 mV (with efficiencies easily exceeding 9.5%, see Table S1, Table S2 and Figure S1 of the S.I., which includes the best, average and standard deviation of the most relevant optoelectronic parameters). Additionally, the J_{SC} exhibits a slight increase while the fill factor (F.F.) and the shunt resistance (R_{SH}) are remarkably increased. This implies that the Ge incorporation in rather small quantities into the CZTSe matrix has an unexpected complex behavior, impacting on several properties of the material.

To better support the electrical characterization of the devices, the dark J-V curves were also analyzed and the diode quality factor (A) and reverse saturation current (J_0) were extracted, together with the band-gap E_G and the ($E_G/q - V_{OC}$) parameters. As is clear, the addition of the Ge superficial nanolayer improves both diode parameters, indicating that the quality of the p-n junction was improved and the carrier recombination in the Ge10 device reduced.

The improvements in the photogenerated current collection are also reflected in the EQE spectra as is shown in **Figure 1**. The EQE is almost unaffected in the 300-620 nm wavelength region being markedly higher for longer wavelengths, indicating an enhanced collection of charge carrier generated deep within the absorber.[14] Additionally, the E_G of the absorbers was estimated with the EQE by the derivative method (see **Figure 1** and Table S1 of S.I.). Clearly, the band-gap is unaffected by Ge, but we must to consider that with these measurements only the effective minimum E_G is obtained. Complementary PL measurements were performed as is shown in Figure S2 of the S.I., showing no changes in the PL spectra in agreement with the almost constant band-gap estimated by EQE. Finally, the $E_G/q - V_{OC}$ (voltage deficit) is also presented, where it is clear that the voltage deficit is reduced for the Ge10 device. In fact, we estimate a value of the voltage deficit of 587 mV, comparable or even better than the best results reported in the literature for the record devices.[3,13,15] Although the origin can be complex, we expect this to be related to an increased diffusion length due to an improved crystalline quality. The questions now are: i. where is the Ge located? and ii. why can such low amount of Ge lead to this large efficiency improvement?

To evaluate the presence of Ge in the absorber we performed TEM and scanning electron microscopy (SEM) studies. Left side of **Figure 2** presents the High-Angle Annular Dark-Field HAADF (Z-contrast) overview of a lamella produced from the Ge10 sample, together with an enlargement of nano-scale features observed in the bulk. After a careful compositional analysis of several representative areas of the lamella (including back and surface interfaces and grain boundaries) with EELS, neither at the surface nor at the back of the CZTSe absorber was Ge detected. Based on the experimental parameters, scattering cross section shape, and equipment used for this experiment, we estimate that the minimum atomic fraction of Ge necessary for detection would be 0.2%, corresponding to a Ge/(Ge+Sn) ratio of 1.6%.[16,17] This is significantly smaller than the 4.4% ratio in the initial precursors. Thus, the V_{OC} increase (up to 469 mV as is shown in the S.I.) is even more impressive taking into account that the absorber can be considered almost Ge-free $Cu_2ZnSnSe_4$. This leads to the conclusion that the V_{OC} increase is not related to a band-gap increase at the surface as was originally assumed.

Analyzing the lamella in detail, we found that the CZTSe absorber layer exhibits an unexpected substructure. This substructure consists of a large number of nanoscale inclusions of a very different chemical composition. These show up as regions of different intensity level in the HAADF (Z-contrast) overview micrograph presented in **Figure 2**. These inclusions appear to be on the order of 1 – 10 nm in diameter and are concentrated around the CZTSe grain boundaries, but it is important to note that some of them were found embedded within large grains as well (it is important to remark that these inclusions are also observed in samples with higher Ge quantities). A more detailed EELS analysis of these nano-structures is presented in the right hand part of **Figure 2**. Clearly, these inclusions are formed by two types of materials. First, GeO_x inclusions with a diameter ranging from some 2 – 5 nm are identified, being the only EELS evidence of the presence of Ge in the layer (see Figure S3 of the S.I. for a detailed description of the evaluation of the nano-structures). Intriguingly, these GeO_x

inclusions appear to be Sn-neutral with respect to the bulk, while they are also clearly Cu, Zn, and Se-poor. On the other hand, SnO_2 inclusions are also observed in the neighbouring areas. Knowing that the Ge appears to form Ge-oxide nano-inclusions, we propose that this may increase the CZTSe grain size through the formation of a liquid phase.

Figure 3 shows comparative cross sectional SEM images of the Ref. and Ge10 solar cells, where large grains and reduced density of grain boundaries are observed in the later. It is important to highlight that these samples are representative for both processes, and were selected among several cross sectional studies (see also Figure S4), supporting the observed improvement of the crystalline quality for the Ge containing samples. To understand this behavior we consider the complex Ge-Se phase diagram. Under the conditions used in our reactive thermal annealing (P=1 bar, T=550 ºC), we expect the Ge precursor layer to form a Ge_3Se_7 phase which melts incongruently at 385 °C and is decomposed into a volatile $GeSe_2$ and a liquid phase with high selenium content (~85 at.% of Se).[18] The liquid phases can assist the crystal growth which offers an explanation for the enlarged grains observed by SEM. The lower density of grain boundaries and associated defects in turn might contribute to a general reduction of recombination paths and an improvement of the solar cells performance. The formation of a volatile $GeSe_2$ phase would lead to a Ge loss as is observed, similar to the well documented Sn loss in kesterite.[19]

The following reaction is then proposed to explain both the crystallization assisted for a Ge liquid phase, and the already observed Ge loss:

$$3Ge_{(s)} + {}^{7}/_{2}\, Se_{2(g)} \leftrightarrow Ge_3Se_{7(s)} \overset{*}{\rightarrow} GeSe_{2(g)} + Ge_xSe_{y(l)}(\sim 85\ at.\%\ Se)$$

Equation 1. Proposed reaction for the formation of a Ge-Se volatile specie ($GeSe_2$) plus a Se-rich liquid phase that assists the absorber crystallization. * This last equation is not equilibrated.

Figure 3 also presents TOF-SIMS in-depth profiles of Ref. and Ge10 samples, confirming the very low Ge concentration throughout the absorber thickness. In particular, the comparison of both samples shows that Cu, Zn and Sn profiles are practically unaffected by the presence of Ge. Apparently, the rather small nominal concentrations used in this work are insufficient to modify the distribution of the cations. According to the TOF-SIMS results, the low Ge signal is mainly concentrated in the top-half part of the sample in agreement with the TEM analysis, which shows that most of the GeO_x nano-inclusions are also in the upper part. In the bottom-half part of the sample, the Ge signal is reduced to the noise level. The Ge amount in the reference sample is below the detection limit.

In addition, a structural analysis of the front and back region was carried out with Raman spectroscopy, which is sensitive to detect little amounts of Ge in the structure (Figure S6 of the S.I.).[20,21] As is observed, the main A^1 mode at the surface region of the Ge10 sample is only slightly blue shifted with respect to the reference sample by only 0.26 cm^{-1}. This shift can be originated by either rather small Ge quantity incorporation in the lattice or the improvement of the crystalline quality.[21,22] By supposing that the shift is completely related to the Sn substitution by Ge, the Ge/(Ge+Sn) ratio in the surface region can be estimated to be lower than 2%. Despite the low Ge incorporation, the decreased FWHM of the A^1 modes recorded at the surface clearly evidences the increased crystalline quality of Ge10. In fact, the observed blue shift of the A^1 mode for the Ge10 sample could also be interpreted as a result of a reduction of the crystal lattice disorder.[22]

The situation is markedly different at the back region of both samples, where very similar Raman shift and FWHMs are obtained suggesting that the Ge surface approach has a limited impact on this region. In fact, combining SEM and TEM analysis we estimate that the $MoSe_2$ thickness is about 80-100 nm independently of the Ge quantity used as capping nanolayer. We therefore conclude that the most important changes introduced by the Ge addition are located at the surface and in the bulk.

Finally, in the S.I. a preliminary XPS characterization of Ref. and Ge10 absorbers is presented (see Figure S7 of S.I.), in order to evaluate the impact of Ge nanolayer in the Sn^{+2} and Sn^{+4} valence states formation. Our first results show a clear shift of the Sn3d5 peak towards higher binding energies when Ge is introduced, suggesting that Sn^{+4} oxidation state prevails over Sn^{+2}. This strongly support that the presence of Ge, prevent in some extent the formation of reduced Sn species like Sn^{+2}, that could be detrimental for the solar cells performance.[6]

In summary, we report here a breakthrough in the kesterite solar cell technology based on the introduction of a nanometric Ge layer, which dramatically improves the solar cells efficiency, from 7% for the reference sample (Ge-free) to 10.1% with an optimized Ge quantity. With a detailed compositional and structural characterization we demonstrate that surprisingly the Ge is barely incorporated into the CZTSe layer, and propose a mechanism how Ge might assist the crystallization via the formation of a liquid phase. A large amount of Ge is expected to be re-evaporated during the decomposition of the Ge_3Se_7 phase. Despite the Ge loss, the remarkable improvement of the device performance can be explained by one or several of the following reasons:

1. The formation of Ge_3Se_7 phase that incongruently decomposes into volatile $GeSe_2$ and a Se-rich liquid phase which assists the crystallization of CZTSe, improving the crystalline quality and helping to obtain large grains.

2. The presence of Ge reduces the probability of formation of Sn-reduced species like Sn^{+2} that are commonly associated to deep defects that deteriorate the cell voltage, as is suggested by preliminary XPS analysis.

3. The only evidence we found for an incorporation of Ge into the CZTSe absorber is the presence of GeO_x nano-inclusions inserted in the grains bulk, apparently associated to the formation of SnO_2 inclusions as well. Although we are analyzing the impact of these nano-

inclusions, one hypothesis under study is that these structures might act as electron back reflectors, which might largely enhance the voltage of the solar cells.

Further investigations on the origin of these effects are currently under way applying advanced characterization methodologies. This communication demonstrates that the application of rather small quantities of Ge onto the CZTSe precursors dramatically increases the voltage and the efficiency of the resulting devices. This opens new paths to strongly reduce the voltage deficit problem of kesterite solar cells, since this methodology can be applied to many different process technologies, leading the way towards high efficiency devices.

Experimental Section

CZTSe absorber synthesis: CZTSe films were prepared by a sequential process onto Mo coated soda lime glass substrates, consisting in a metallic stack deposition followed by a reactive annealing process. Cu/Sn/Cu/Zn metallic stacks were tuned in order to obtain Zn-rich and Cu-poor conditions (Cu/(Zn+Sn) = 0.75 and Zn/Sn = 1.20 determined with a calibrated X-ray fluorescence (XRF, Fischerscope XVD)) and deposited using DC magnetron sputtering (Alliance Ac450), as has been reported elsewhere.[10] Additionally, Ge nano-layers with different thicknesses were thermally evaporated on top of the precursors (1, 2, 5, 10, 15 and 25 nm, Oerlikon Univex 250). The whole precursor stack (5x5 cm^2 in area) was subsequently annealed in a Se+Sn containing atmosphere (100 mg of Se –Alfa-Aesar powder, 200 mesh, 99.999%- and 5 mg of Sn –Alfa-Aesar powder, 100 mesh, 99.995%), using graphite boxes (69 cm^3 in volume) in a conventional tubular furnace. The selenization was performed in a 2-step process, the first one at 400 ºC (heating ramp 20 ºC/min) during 30 min and 1.5 mbar Ar pressure, followed by the second step at 550 ºC (heating ramp 20 ºC/min) during 15 min and 1 bar Ar pressure, with a natural cooling down to room temperature.

Solar cell fabrication: To complete the devices, a CdS buffer layer (50 nm) was deposited by chemical bath deposition (CBD), preceded by several chemical etchings in order to remove secondary phases on the surface of the absorber and to passivate it.[13,23] Firstly, an oxidizing etching was performed by using $KMnO_4$ + H_2SO_4 solution, followed by a chemical etching in $(NH4)_2S$ solution, and finally a diluted KCN solution was used to etch the absorber.[23,24] Immediately after CdS growth, the solar cells were completed by DC-pulsed sputtering deposition of i-ZnO (50 nm) and In_2O_3-SnO_2 (ITO, 350 nm) as transparent conductive window layer (Alliance CT100). Afterwards, for the optoelectronic characterization, 3 x 3 mm^2 cells were mechanically scribed using a manual microdiamond scriber MR200 OEG. Neither anti-reflecting coating, nor metallic grids were used for the optoelectronic characterization of the devices.

Film and device characterization: Dark and illuminated J-V curves were measured using a calibrated Sun 3000 class AAA solar simulator (Abet Technologies, 25 ºC, AM1.5G illumination). The spectral response was measured using a Bentham PVE300 system calibrated with Si and Ge photodiodes, in order to obtain the external quantum efficiency (EQE) of the solar cells. Transmission electron microscopy (TEM) analysis were carried out using a Tecnai F30 from FEI company operated at 300 kV and equipped with a Tridiem image filter from Gatan, Inc for Electron Energy-Loss Spectrometry (EELS) measurements. The lamellae were prepared for TEM investigation using the Focused Ion Beam (FIB) in-situ lift-out method and thinned to a final thickness of less than 100 nm using a 5 kV Ga+ beam. The sample preparation method that we employed is particularly well-suited to correlating macroscale behavior to nanoscale effects (we had more than 10 µm of the full stack in cross-section available). SEM images were obtained with a ZEISS Series Auriga microscope using 5 kV accelerating voltage. Raman spectra were obtained using a Horiba Jobin Yvon LabRam

HR800-UV coupled with an Olympus metallographic microscope. Backscattering measurements were performed using a 532nm excitation wavelength (penetration depth below 100 nm). All Raman measurements were carried-out in an area of 30x30 μm^2 in a dual-scan mode. The laser spot diameter was about 1 µm. For avoiding possible thermal effects in the Raman experiments the power density was kept below 16 kW/cm^2. The Raman spectra have been calibrated using a Si monocrystal reference and imposing the Raman shift for the main Si band at 520 cm^{-1}. In order to evaluate the Raman shift and FWHM errors several Raman experiments on the same position of the samples were performed. The same set-up was used to record the PL spectra of the samples. TOF-SIMS measurements were performed in an ION-TOF IV equipment, equipped with 25kV Bi cluster primary ion gun for analysis, and O_2 and Cs ion guns for sputtering in depth profiling modes. The analyzed area was 50 µm x 50 µm with a cycle time of 100 µs and a time to digital converter (TDC) resolution of 200 ps. XPS measurements were performed in a PHI 5500 Multitechnique System (from Physical Electronics) with a monochromatic X-ray source (Aluminium Kα line of 1486.6 eV energy and 350 W), placed perpendicular to the analyzer axis and calibrated using the 3d5/2 line of Ag with a full width at half maximum (FWHM) of 0.8 eV.

Supporting Information
Supporting Information is available from the Wiley Online Library or from the author.

Acknowledgements
This research was supported by the Framework 7 program under the project KESTCELLS (FP7-PEOPLE-2012-ITN-316488), by MINECO (Ministerio de Economía y Competitividad de España) under the SUNBEAM project (ENE2013-49136-C4-1-R) and NOVACOST project (PCIN-2013-128-C02-01) and by European Regional Development Founds (ERDF, FEDER Programa Competitivitat de Catalunya 2007–2013). Authors from IREC and the University of Barcelona belong to the M-2E (Electronic Materials for Energy) Consolidated Research Group and the XaRMAE Network of Excellence on Materials for Energy of the "Generalitat de Catalunya". SG thanks the Government of Spain for the FPI fellowship (BES-2014-068533), Y.S. for the PTA fellowship (PTA2012-7852-A), M.P. for the MINECO postdoctoral fellow (FPDI-2013-18968), and E.S. for the "Ramón y Cajal" fellowship (RYC-2011-09212). H.X. thanks the "China Scholarship Council" fellowship (CSC Nº 201206340113). P.P. The European Union for the JUMPKEST Marie Curie Individual Fellow (FP7-PEOPLE-2013-IEF- 625840).

Received: ((will be filled in by the editorial staff))
Revised: ((will be filled in by the editorial staff))
Published online: ((will be filled in by the editorial staff))

[1] S. Siebentritt, S. Schorr, *Prog. Photovolt. Res. Appl.* **2012**, *20*, 512.

[2] D. B. Mitzi, O. Gunawan, T. K. Todorov, D. A. R. Barkhouse, *Phil. Trans. R. Soc. A* **2013**, *371*, 20110432.

[3] Y. S. Lee, T. Gershon, O. Gunawan, T. K. Todorov, T. Gokmen, Y. Virgus, S. Guha, *Adv. Energy Mater.* **2014**, *5*, 1401372.

[4] T. K. Todorov, K. B. Reuter, D. B. Mitzi, *Adv. Mater.* **2010**, *22*, 1.

[5] S. Bag, O. Gunawan, T. Gokmen, Y. Zhu, D. B. Mitzi, *Chem. Mater.* **2012**, *24*, 4588.

[6] C. J. Hages, S. Levcenco, C. K. Miskin, J. H. Alsmeier, D. Abou-Ras, R. G. Wilks, M. Bär, T. Unold, R. Agrawal, *Prog. Photovolt. Res. Appl.* **2013**, *23*, 376.

[7] I. Kim, K. Kim, Y. Oh, K. Woo, G. Cao, S. Jeong, J. Moon, *Chem. Mater.* **2014**, *26*, 3957.

[8] T. J. Huang, X. Yin, G. Qi, H. Gong, *Phys. Status Solidi RRL* **2014**, *8*, 735.

[9] K. Biswas, S. Lany, A. Zunger, *Appl. Phys. Lett.* **2010**, *96*, 201902.

[10] A. Fairbrother, X. Fontané, V. Izquierdo-Roca, M. Placidi, D. Sylla, M. Espindola-Rodriguez, S. López-Mariño, F. A. Pulgarín, O. Vigil-Galán, A. Pérez-Rodríguez, E. Saucedo, *Prog. Photovolt. Res. Appl.* **2014**, *22*, 479.

[11] M. Grossberg, K. Timmo, T. Raadik, E. Kärber, V. Mikli, J. Krustok, *Thin Solid Films* **2014**, *582*, 176.

[12] V. Fthenakis, *Renew. Sustain. Ener. Rev.* **2009**, *13*, 2746.

[13] M. Neuschitzer, Y. Sánchez, S. López-Marino, H. Xie, A. Fairbrother, M. Placidi, S. Haass, V. Izquierdo-Roca, A. Pérez-Rodríguez, E. Saucedo, *Prog. Photovolt. Res. Appl.*, DOI: 10.1002/pip.2589.

[14] G. Brown, V. Faifer, A. Pudov, S. Anikeev, E. Bykov, M. Contreras, J. Wu, *Appl. Phys. Lett.* **2010**, *96*, 022104.

[15] T. K. Todorov, J. Tang, S. Bag, O. Gunawan, T. Gokmen, Y. Zhu, D. B. Mitzi, *Adv. Energy Mater.* **2012**, 3, 34; and W. Wang, M. T. Winkler, O. Gunawan, T. Gokmen, T. K. Todorov, Y. Zhu, D. B. Mitzi, *Adv. Energy Mater.* **2014**, 4, 1301465.

[16] R.F. Egerton, *Electron energy-loss spectroscopy in the electron microscope*, Springer, New York, USA **2011**.

[17] K. Riegler, G. Kothleitner, *Ultramicroscopy* **2010**, *110*, 1004.

[18] S. Stølen, H. B. Johnsen, C. S. Bøe, O. B. Karlsen, T. Grande, *J. Phase Equilibria* **1999**, *20*, 17.

[19] A. Redinger, D.M. Berg, P.J. Dale, S. Siebentritt, *J. Am. Chem. Soc.* **2011**, *133*, 3320.

[20] D. B. Khadka, J. Kim, *J. Phys. Chem. C* **2015**, *119*, 1706.

[21] M. Dimitrievska, A. Fairbrother, A. Pérez-Rodríguez, E. Saucedo, V. Izquierdo-Roca, *Acta Materialia* **2014**, *70*, 272.

[22] R. Caballero, J. M. Cano-Torres, E. Garcia-Llamas, X. Fontané, A. Pérez-Rodríguez, D. Greiner, C. A. Kaufmann, J. M. Merino, I. Victorov, G. Baraldi, M. Valakh, I. Bodnar, V. Izquierdo-Roca, M. León, *Solar Energy Mater. Solar Cells* **2015**, *139*, 1.

[23] S. López-Marino, Y. Sánchez, M. Placidi, A. Fairbrother, M. Espindola-Rodríguez, X. Fontané, V. Izquierdo-Roca, J. López-García, L. Calvo-Barrio, A. Pérez-Rodríguez, E. Saucedo, *Chem.–Eur. J.* **2013**, *19*, 14814.

[24] H. Xie, Y. Sánchez, S. López-Marino, M. Espíndola-Rodríguez, J. López-García, M. Neuschitzer, D. Sylla, A. Fairbrother, A. Pérez-Rodríguez, E. Saucedo, *ACS Appl. Mater. Interfaces* **2014**, *6*, 12744.

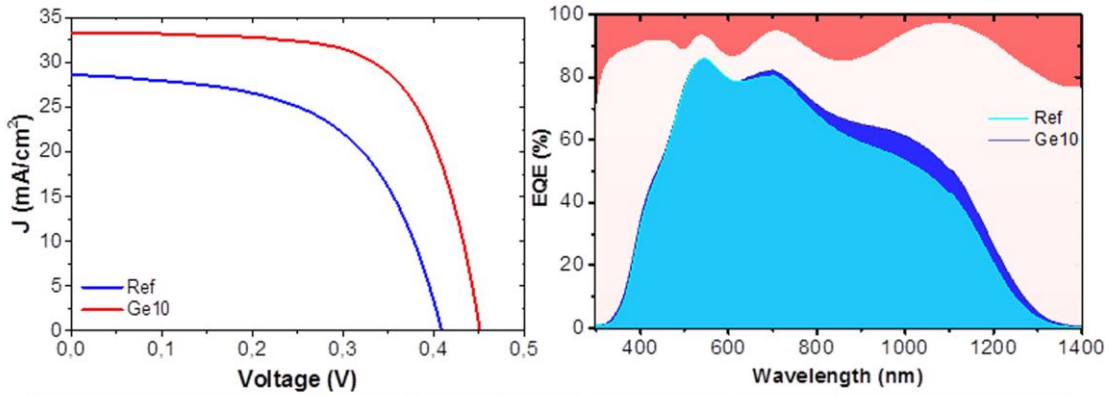

Sample	V_{OC} (mV)	J_{SC} (mA/cm^2)	FF (%)	Eff (%)	R_s (Ω·cm^2)	R_{sh} (Ω·cm^2)	A	J_0 (mA/cm^2)	E_G (eV)	$E_G/q - V_{OC}$ (eV)
Ref	408	29.1	59.2	7.0	0.23	265	1.86	9.9×10^{-3}	1.04	0.632
Ge10	453	33.3	66.8	10.1	0.52	712	1.70	6×10^{-4}	1.04	0.587

Figure 1. J-V curves and the corresponding optoelectronic parameters of reference and Ge10 solar cells (left hand); and EQE plot of both samples (right hand). In the EQE plot, the upper orange area represents the reflectance of both solar cells.

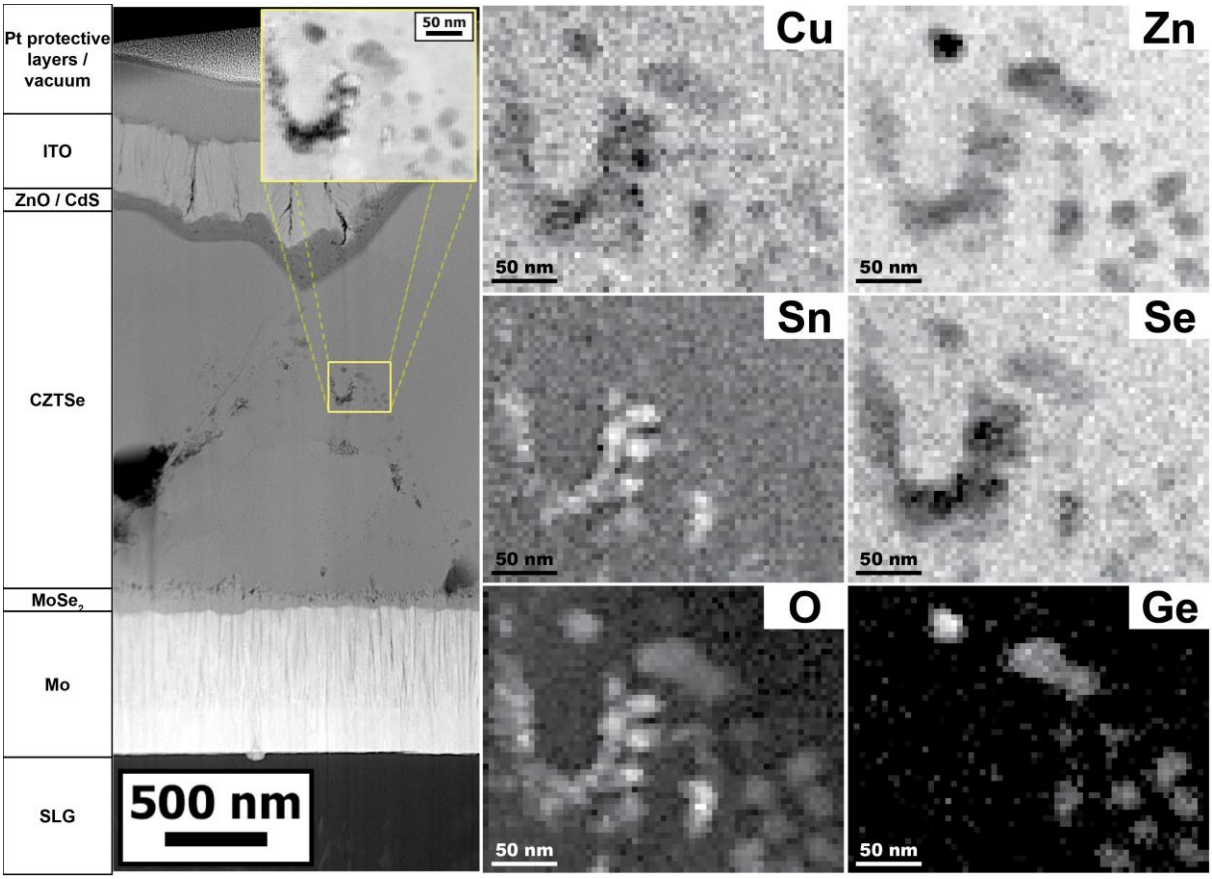

Figure 2. TEM/EELS analysis of Ge10 sample. High-Angle Annular Dark-Field HAADF (Z-contrast) overview of the lamella (left hand). EELS analysis of the nano-structures observed in the TEM image, including the signal of Cu, Zn, Sn, Se, O and Ge (right hand).

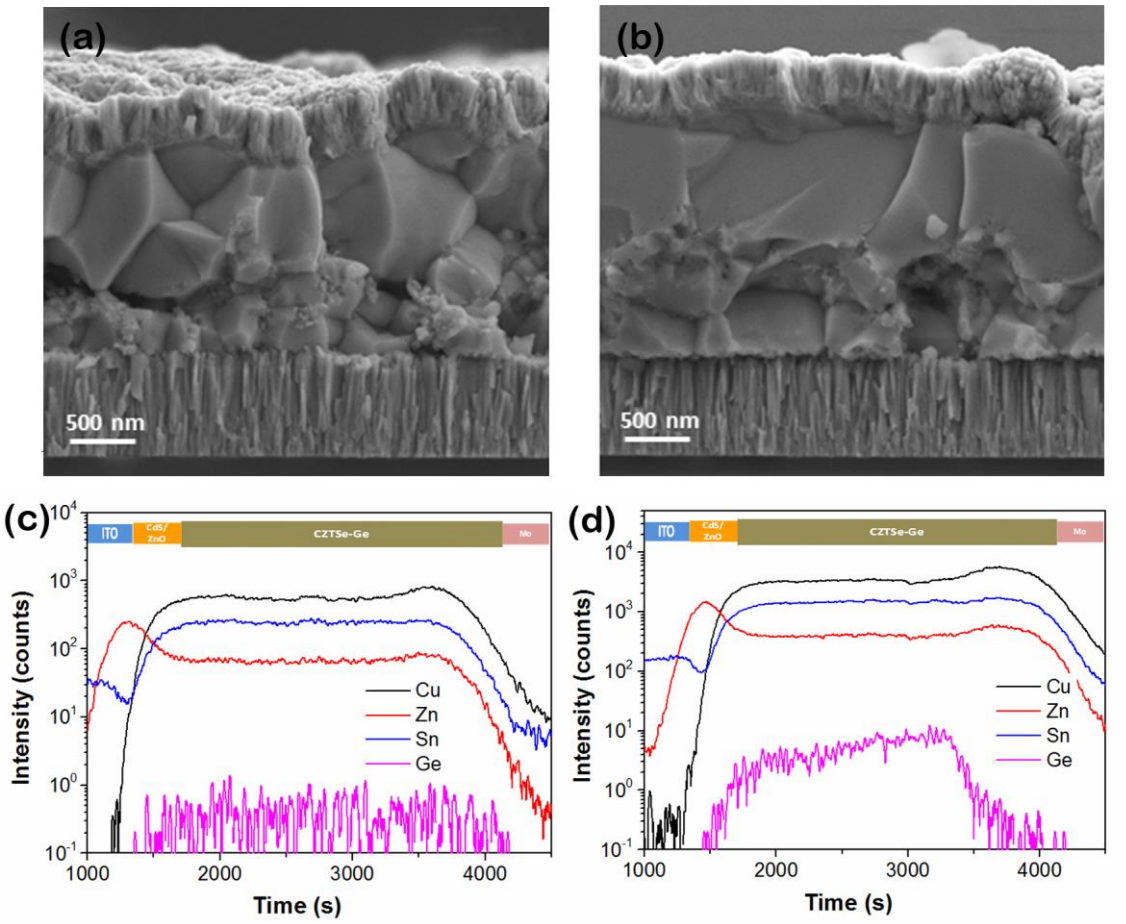

Figure 3. Comparative cross sectional SEM views of Ref. (a) and Ge10 (b) samples. TOF-SIMS profile of Ref (c) and Ge10 (d) samples, showing the metallic in-depth distribution.

A large improvement of $Cu_2ZnSnSe_4$ solar cells efficiency is presented based on the introduction of a Ge superficial nano-layer. This improvement is explained by three complementary effects: the formation of a liquid Ge-related phase, the possible reduction of Sn multi charge states and the formation of GeO_2 nano-inclusions, which lead to an impressive solar cell V_{OC} increase. (Figures in the graphical abstract are artwork created from real SEM figures)

Keywords: $Cu_2ZnSnSe_4$, Ge nano-layer, Kesterite, thin film solar cells

S. Giraldo, M. Neuschitzer, T. Thersleff, S. López-Marino, Y. Sánchez, H. Xie, M. Colina, M. Placidi, P. Pistor, V. Izquierdo-Roca, K. Leifer, A. Pérez-Rodríguez, and E. Saucedo* Corresponding Author*

Large efficiency improvement in $Cu_2ZnSnSe_4$ solar cells by introducing a superficial Ge nano-layer